Solid State Phenomena
ISSN: 1662-9779, Vol. 312, pp 200-205

Submitted: 2020-04-28
Accepted: 2020-06-01
Online: 2020-11-11

Pulsed Laser Ablation of Silicon Nanowires in Water and Ethanol

Stanislav V. Zabotnov[1,a*], Anastasiia V. Skobelkina[1,b], Fedor V. Kashaev[1,c], Aleksandr V. Kolchin[1,d], Vladimir V. Popov[1,e], Denis E. Presnov[1,2,3,f], Ekaterina A. Sergeeva[4,1g], Mikhail Yu. Kirillin[4,h] and Leonid A. Golovan[1,i]

[1]Faculty of Physics, Lomonosov Moscow State University, 1/2 Leninskie Gory, Moscow, 119991, Russia

[2]Skobeltsyn Institute of Nuclear Physics, Lomonosov Moscow State University, 1/2 Leninskie Gory, Moscow, 119991, Russia

[3]Quantum Technology Centre, Lomonosov Moscow State University, 1/35 Leninskie Gory, Moscow, 119991, Russia

[4]Institute of Applied Physics RAS, 46 Uljanov St., Nizhny Novgorod, 603950, Russia

[a*]zabotnov@physics.msu.ru, [b]snastya.19996@mail.ru, [c]kashaev.fedor@gmail.com, [d]avkolchin@physics.msu.ru, [e]vvpopov@physics.msu.ru, [f]denis-presnov@yandex.ru, [g]sea_nnov@yahoo.com, [h]mkirillin@yandex.ru, [i]golovan@physics.msu.ru

Keywords: pulsed laser ablation in liquids, silicon nanowires, silicon nanoparticles, ablation threshold, Raman spectroscopy

Abstract. A novel two-stage technique to fabricate silicon nanoparticles is reported. At the first stage, silicon nanowire arrays are formed by metal-assisted chemical etching. At the second stage, the nanoparticles are produced by pulsed laser ablation of the silicon nanowire targets in water and ethanol. The fabricated particles have relatively small mean size in the range of 24 – 45 nm depending on the used buffer liquid. The ablation threshold of the silicon nanowire arrays is 2 – 11 times smaller than that for crystalline silicon targets. Owing to the achieved parameters, the proposed technique is more efficient in comparison with traditional approaches of mechanical milling of silicon nanowires and laser ablation of crystalline silicon. Raman spectroscopy study revealed crystalline structure of the fabricated silicon nanoparticles. The properties of the produced nanoparticles indicate their high potential of in biophotonics.

Introduction

Pulsed laser ablation of solid-state targets in different liquids and gases is a powerful modern tool to produce a variety of nanoparticles with desirable size, physical and chemical properties [1]. Silicon nanoparticles (Si-NPs) produced by this technique have potential in such biomedical applications as fluorescence imaging [2], photodynamic therapy [3], optical coherence tomography [4] and tissue engineering [5] due to high biocompatibility and biodegradability of nanostructured silicon [6, 7].

Among other advantages of the pulsed laser ablation technique, capacities for fabrication of Si-NPs with a wide range of available sizes [1, 8] and high chemical purity [3] are to be highlighted. The main drawback of this technique consists in a relatively low Si-NPs output as compared to chemical etching and mechanical milling of silicon. High-yield production of Si-NPs is quite time-consuming and requires employment of a powerful laser with the high repetition rate.

To overcome this limitation, we suggested a novel two-stage technique of Si-NPs fabrication [9]. At the first stage, porous silicon matrices are formed by chemical etching. At the second stage, the Si-NPs are produced by pulsed laser ablation in liquids (PLAL) using the porous targets obtained at the first stage. The porous structure of the targets promotes Si-NPs generation with higher efficiency in comparison with the use of crystalline silicon as a target.

Earlier this approach has demonstrated its efficiency with the porous silicon targets fabricated by electrochemical etching [9]. In this paper we study structural properties of laser-ablated Si-NPs

produced from silicon nanowires (Si-NWs) arrays targets fabricated by metal-assisted chemical etching (MACE) [10].

Materials and Methods

Formation of Silicon Nanowire Arrays. The MACE technique was employed to fabricate Si-NW arrays that further serve as targets for laser ablation. Two types of (100) crystalline silicon boron-doped wafers were chosen as initial samples for etching: low-doped wafers with the specific resistivity of 12 Ohm·cm and heavily-doped wafers with the specific resistivity of 10 – 20 mOhm·cm. Preliminary all wafers were rinsed in 49% hydrofluoric acid (HF) for 1 minute to remove surface oxide. Further, Ag nanoparticles were deposited on the silicon wafers by means of dipping the samples into a solution (1:1) of 0.02 M $AgNO_3$ in water and 5 M HF for 30 seconds. At the next step, the silver covered wafers were dipped into a solution (10:1) of 5 M HF and 30% hydrogen peroxide (H_2O_2) for 40 minutes. To remove the silver nanoparticles after etching all samples were placed into 65% nitric acid (HNO_3) for 15 minutes and later rinsed with water.

Nanoparticle fabrication via PLAL. Irradiation of the Si-NW arrays was performed in a 15 ml cell [8] filled by distilled water or ethanol using an EKSPLA PL 2143A picosecond Nd:YAG laser during 30 min with a pulse repetition rate of 10 Hz. The duration, wavelength and energy of the pulses were 34 ps, 1064 nm and 10 mJ, respectively.

The laser beam was focused onto a layer of the Si-NWs by a lens with the focal distance of 40 mm at the normal incidence. To prevent degradation of the targets during PLAL, the cell was shifted perpendicular to the axis of the laser beam using two orthogonally oriented automated mechanical translation stages.

Analysis of Structural Properties. Structural properties of Si-NWs were studied using a Carl Zeiss Supra 40 scanning electron microscope (SEM) and a ND-MDT SolverPRO scanning probe microscope. Raman spectra were measured by a Horiba Jobin Yvon HR 800 spectrometer with excitation by Ar laser at the wavelength of 488 nm.

Ablation Threshold Measurements. To measure the ablation threshold value, we used the method described in [11]. The essence of the approach consists in measuring the dependence of the crater diameter D on the pulse energy E. The samples were irradiated in a single pulse mode with pulse energy E varied in the range of 0.3 – 5 mJ. The crater diameter D after irradiation was measured using an Olympus BX41 microscope. The dependences of D^2 on pulse energy E were further extrapolated with logarithmic approximation to obtain the threshold energy E_{th} at zero value of D^2 according to the expression:

$$D^2 = 2w_0^2 \ln(E/E_{th}), \quad (1)$$

where $2w_0^2$ is $1/e^2$ radius of the Gaussian beam. As a result, the threshold energy fluence F_{th} may be calculated as:

$$F_{th} = 2E_{th}/\pi w_0^2. \quad (2)$$

Results and Discussion

Typical SEM images of the fabricated Si-NW arrays prior to laser irradiation are presented on Fig. 1a,b. All wires are oriented perpendicular to surface due to using (100) Si wafers [10]. The Si-NW arrays have thickness of 25±4 μm and 10±2 μm for low-doped and heavily-doped wafers, respectively. Below these samples are referred to as LD Si-NWs and HD Si-NWs, correspondingly. The difference between the acquired thicknesses for the same etching time is in a good correlation with previous works where LD Si-NWs [10] and HD Si-NWs [12] were studied. Another difference is a tendency of the heavily-doped nanowires top ends towards convergence (Fig. 1b) in contrast to the separated low-doped wires (Fig. 1a). We assume the existence of a relatively strong electrostatic

forces in the structures with heavily doping. The diameter of Si-NWs is in the range of 100 – 200 nm for both types of Si-NWs.

After PLAL, SEM studies revealed that all ablation craters have round shape (see example in Fig. 1c) and ablation occurs only within the Si-NW layers, while crystalline silicon substrates remain unmodified. The dependencies of the crater diameter squared D^2 on the laser pulse energy E are close to logarithmic for all samples (see example in Fig. 2).

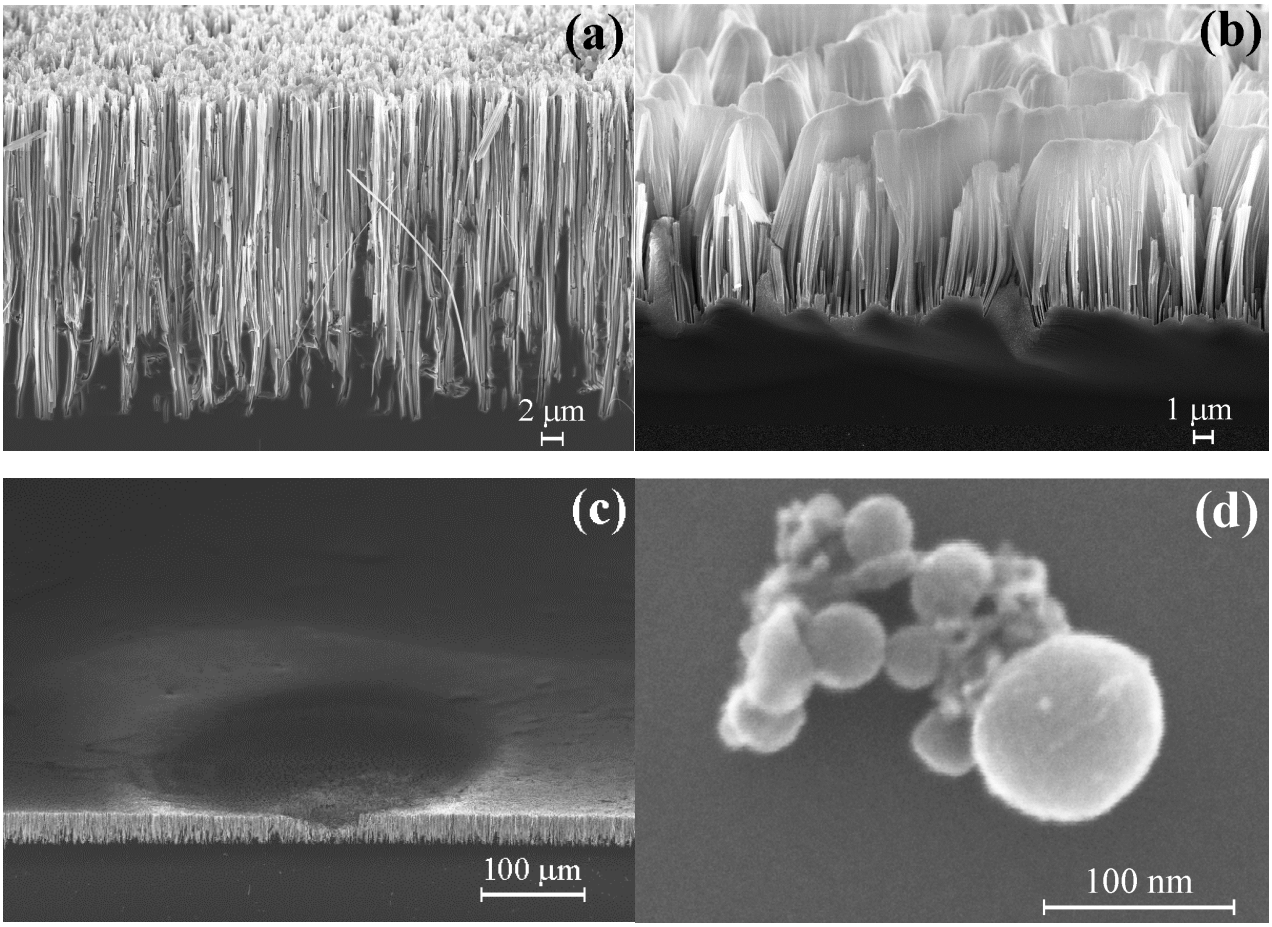

Fig 1. SEM images of (a) LD Si-NWs, (b) HD Si-NWs, (c) crater after laser ablation (E = 0.3 mJ) of LD Si-NWs in water, (d) Si-NPs produced by laser ablation of LD Si-NWs in water.

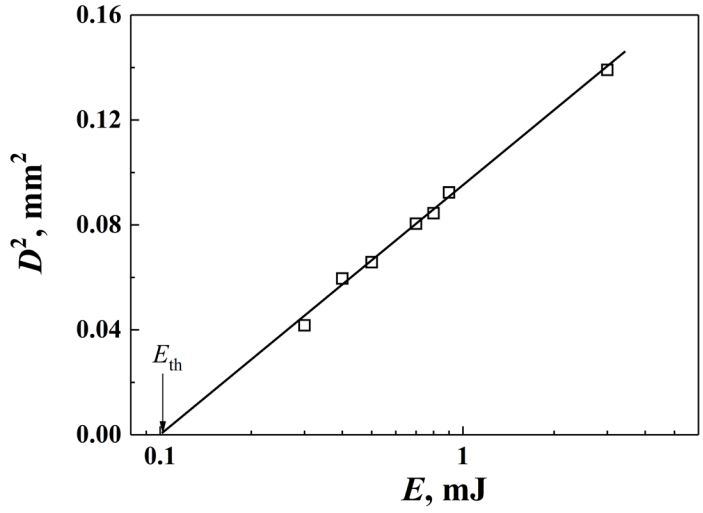

Fig 2. Typical dependence of the crater diameter squared D^2 on the laser pulse energy E for case of single pulse laser ablation of HD Si-NWs in water.

The values of ablation threshold energy fluence calculated using Eqs. (1) and (2) are presented in Table 1. Besides ablation of Si-NWs in water and ethanol, the results for crystalline silicon ablation in the same liquids are given for reference.

Table 1. Ablation threshold energy fluences.

Buffer medium	F_{th} for LD Si-NWs [J/cm^2]	F_{th} for HD Si-NWs [J/cm^2]	F_{th} for crystalline Si [J/cm^2]
Water	0.158±0.013	0.32±0.01	1.26±0.11
Ethanol	0.55±0.05	0.104±0.019	1.18±0.09

The obtained ablation thresholds of crystalline silicon in liquids are close to ones reported in paper [11]. The values of threshold energy fluencies for LD Si-NWs and HD Si-NWs are 2 – 11 times smaller than those for crystalline Si. We did not reveal a dominate mechanism of such behavior. We assume that several factors may affect this difference: (i) a lower thermal conductivity of Si-NW matrix as compared to bulk silicon, (ii) partial destruction of Si – Si bonds in the crystal lattice as a result of MACE, (iii) dependence on the buffer medium for ablation, (iv) difference between LD Si-NWs and HD Si-NWs. In the latter case, the Si-NWs have additional inner pores [12]. The revealed decrease of the ablation threshold indicates more effective generation of the Si-NPs in Si-NWs layers as compared to crystalline Si.

SEM study of the laser-ablated Si-NPs revealed their spherical symmetry and sizes primarily smaller than 100 nm for all types of the wafers and buffer liquids (see example in Fig. 1d). More detailed analysis of atomic force microscopy (AFM) data allowed to obtain particle size distributions presented in Fig. 3.

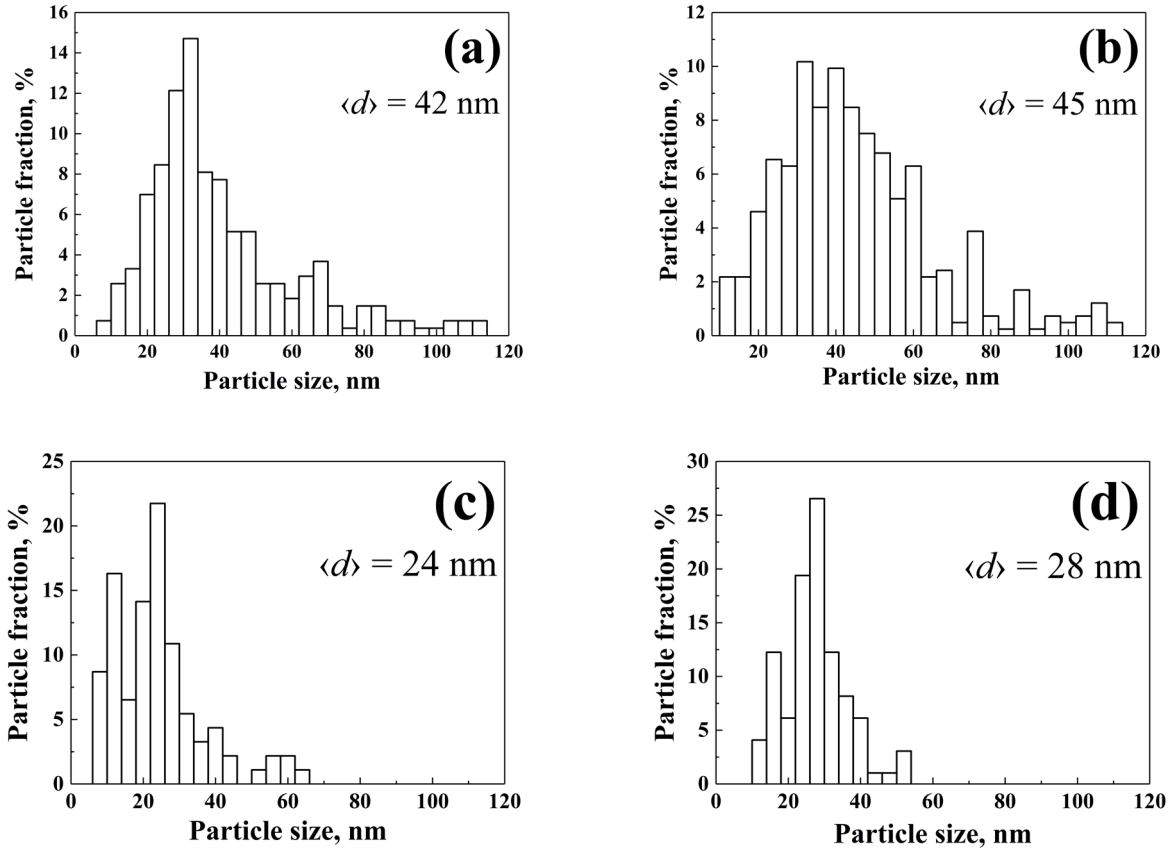

Fig 3. Size distributions for the Si-NPs fabricated via laser ablation of (a) LD Si-NWs in water, (b) HD Si-NWs in water, (c) LD Si-NWs in ethanol, (d) HD Si-NWs in ethanol.

The Si-NPs mean size is referred to as ‹*d*› in Fig. 3 and does not exceed 45 nm for all considered cases. The obtained size distributions demonstrate stronger dependence on the applied buffer liquid

as compared to that on doping level of the employed target. The noticeable effect of used buffer medium on Si-NPs size was registered in our previous studies on PLAL of monocrystalline [8] and porous silicon [9]. In this study we observe a similar tendency: the Si-NPs size is mainly determined by agglomeration efficiency of ablation products due to their deceleration by collisions with molecular environment of the buffer liquid. From the practical point of view, the obtained result is promising, since in biomedical applications the small size of the Si-NPs promotes their better penetration in living organisms.

Raman spectroscopy study revealed a difference in structural features of the samples before and after PLAL. Before laser ablation, Raman spectra of the Si-NWs feature an asymmetric peak (Fig. 4a), which can be considered as a linear combination of two overlapping Raman lines close to 520 cm^{-1} and 510 cm^{-1}. The line close to 520 cm^{-1} corresponds to crystalline silicon. The line close to 510 cm^{-1} was observed in Si-NWs earlier [14 – 16] and is explained by phonon confinement in Si nanocrystals with size of several nanometers as well as by mechanical stresses in crystalline lattice. However, we do not expect the presence of the small nanocrystals in great numbers within the Si-NWs arrays, which is additionally confirmed by the SEM data (Fig. 1a,b). Most likely, the observed red shifted Raman line near 510 cm^{-1} is determined by tensile strain, which is in accordance with paper [16]. Therefore, the nonirradiated Si-NW arrays consist of two fractions: unstrained and strained crystalline silicon. We suppose the strain originates from non-uniform MACE process. A supplementary evidence of this hypothesis consists in the convergence of HD Si-NWs ends due to the stresses (Fig. 1b) in addition to the mentioned above electrostatic forces influence.

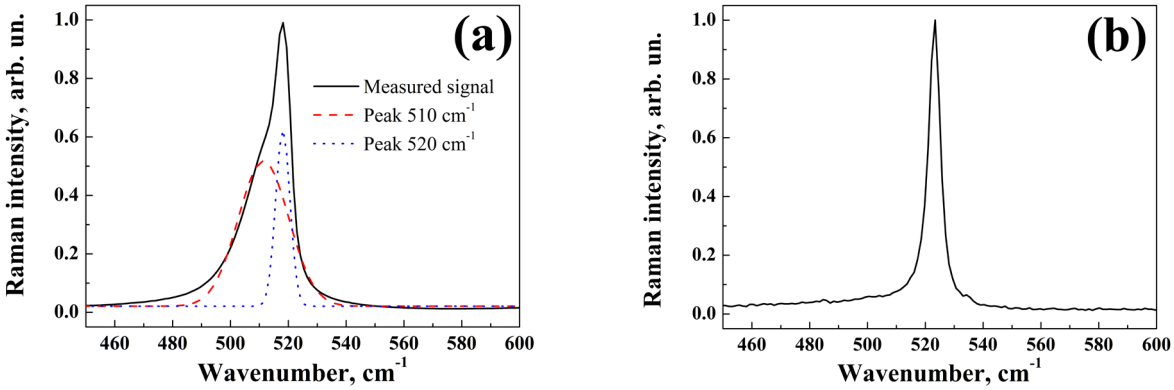

Fig 4. Raman spectra of (a) initial LD Si-NWs and (b) Si-NPs produced by laser ablation of LD Si-NWs in ethanol.

The laser-ablated Si-NPs are characterized by Raman line 520 cm^{-1} only (Fig. 4b), which allows to suppose that the strains disappear as a result of laser ablation. Therefore, the fabricated Si-NPs demonstrate a high crystallinity level. This result demonstrates higher purity of the produced Si-NPs in comparison to the case of laser ablation of porous silicon in similar conditions, for which broad Raman peak near 480 cm^{-1} was detected and corresponding it amorphous silicon phase presence was revealed [17].

Summary

In this paper we report on an approach for forming Si-NPs via laser ablation of the Si-NW arrays in water and ethanol. The mean size of the obtained particles varies in the range of 24 – 45 nm depending primarily on the used buffer liquid. At the same time, the ablation threshold energy fluence additionally depends on the doping level of initial silicon wafer. The ablation threshold of the Si-NW arrays is 2 – 11 times smaller than that for crystalline silicon targets due to a lower thermal conductivity and partial destruction of Si – Si bonds in the Si-NW arrays. The relatively small size and low ablation threshold provide advantages of Si-NPs fabrication via PLAL of the Si-NWs as compared to traditionally used mechanical milling of porous silicon or Si-NWs and laser ablation of

crystalline silicon, respectively. The revealed crystalline structure of the fabricated Si-NPs may enhance their fluorescence and scattering properties and indicates the potential of the fabricated nanoparticles as contrasting agents in biophotonic applications.

This work was supported by the Russian Science Foundation (Grant No. 19-12-00192).

References

[1] D. Zhang, B. Gökce, S. Barcikowski, Laser synthesis and processing of colloids: fundamentals and applications, Chem. Rev. 117 (2017) 3990-4103.

[2] M.B. Gongalsky, L.A. Osminkina, A. Pereira, et al., Laser-synthesized oxide-passivated bright Si quantum dots for bioimaging, Sci. Rep. 6 (2016) 24732.

[3] D. Rioux, M. Laferriere, A. Douplik, et al., Silicon nanoparticles produced by femtosecond laser ablation in water as novel contamination-free photosensitizers, J. Biomed. Opt. 142 (2009) 021010.

[4] S.V. Zabotnov, F.V. Kashaev, D.V. Shuleiko, et al., Silicon nanoparticles as contrast agents in the methods of optical biomedical diagnostics, Quantum Electron. 47 (2017) 638-646.

[5] A. Al-Kattan, V.P. Nirwan, A. Popov, et al., Recent advances in laser-ablative synthesis of bare Au and Si nanoparticles and assessment of their prospects for tissue engineering applications, Int. J. Mol. Sci. 19 (2018) 1563.

[6] O.I. Ksenofontova, A.V. Vasin, V.V. Egorov, et al., Porous silicon and its applications in biology and medicine, Tech. Phys. 59 (2014) 66-77.

[7] J.-H. Park, L. Gu, G. von Maltzahn, et al., Biodegradable luminescent porous silicon nanoparticles for in vivo applications, Nat. Mater. 8 (2009) 331-336.

[8] P.A. Perminov, I.O. Dzhun, A.A. Ezhov, et al., Creation of silicon nanocrystals using the laser ablation in liquid, Las. Phys. 21 (2011) 801-804.

[9] S.V. Zabotnov, D.A. Kurakina, F.V. Kashaev, et al., Structural and optical properties of nanoparticles formed by laser ablation of porous silicon in liquids: Perspectives in biophotonics, Quantum Electron. 50 (2020) 69-75.

[10] V.A. Sivakov, G. Brönstrup, B. Pecz, et al., Realization of vertical and zigzag single crystalline silicon nanowire architectures, J. Phys. Chem. C 114 (2010) 3798-3803.

[11] I.N. Saraeva, S.I. Kudryashov, A.A. Rudenko, et al., Effect of fs/ps laser pulsewidth on ablation of metals and silicon in air and liquids, and on their nanoparticle yields, Appl. Surf. Sci. 470 (2019) 1018-1034.

[12] L.A. Osminkina, V.A. Sivakov, G.A. Mysov, et al., Nanoparticles prepared from porous silicon nanowires for bio-imaging and sonodynamic therapy, Nanoscale Res. Lett. 9 (2014) 463.

[13] S.V. Zabotnov, M.M. Kholodov, V.A. Georgobiani, et al., Photon lifetime correlated increase of Raman scattering and third-harmonic generation in silicon nanowire arrays, Las. Phys. Lett. 13 (2016) 035902.

[14] H. Gebavi, D. Ristić, N. Baran, et al., Silicon nanowires as sensory material for surface-enhanced Raman spectroscopy, Silicon 11 (2019) 1151-1157.

[15] R. Ghosh, P.K. Giri, K. Imakita and M. Fujii, Origin of visible and near-infrared photoluminescence from chemically etched Si nanowires decorated with arbitrarily shaped Si nanocrystals, Nanotechnology 25 (2014) 045703.

[16] R.-P. Wang, G.-W. Zhou, Y.-L. Liu, et al., Raman spectral study of silicon nanowires: High-order scattering and phonon confinement effects, Phys. Rev. B 61 (2000) 16827-16832.

[17] S.V. Zabotnov, A.V. Kolchin, F.V. Kashaev, et al., Structural analysis of nanoparticles formed via laser ablation of porous silicon and silicon microparticles in water, Tech. Phys. Lett. 45 (2019) 1085-1088.